VOLUME 68, NUMBER 6 JOC Articles MARCH 21, 2003

Computer-Aided Design of Chiral Ligands. Part 2. Functionality Mapping as a Method To Identify Stereocontrol Elements for Asymmetric Reactions

Marisa C. Kozlowski* and Manoranjan Panda

Department of Chemistry, Roy and Diana Vagelos Laboratories, University of Pennsylvania, Philadelphia, Pennsylvania 19104

marisa@sas.upenn.edu

Received June 12, 2002

A computational method to determine the energetically favorable positions of functional groups with respect to the transition states of stereoselective reactions based on force field energy minimization is presented. The parameters of this functionality mapping, the characteristics of the target transition states, and the features of the probe structures are outlined. Our method was found to reproduce the positions of the stereodiscriminating fragments for some known chiral ligands including the Masamune dimethylborolane, dimenthylborane, the Corey stien reagent, the Roush allylboronate tartrates, and the secondary amine Diels−Alder catalysts described by MacMillan. Functionality mapping can be used to better understand the specific interactions in the transition states leading to the products by providing a quantitative measure of the stabilization/destabilization afforded by the different ligand components via nonbonded interactions. The method can determine if a chiral ligand imparts the observed selectivity by stabilizing one reaction pathway, by destabilizing a reaction pathway, or by a combination of both. Orientational as well as positional information about potential functional groups is readily obtained. In addition to its utility as an analytical tool, functionality mapping can be used to explore starting points for the design of new chiral ligands.

Introduction

Several studies have been reported on the mapping of suitable functional groups against the active sites of biologically important molecules.[1,2] Determining the energetically favorable positions of functional groups in the binding sites of proteins of known three-dimensional structure not only sheds light on the interaction of these proteins with other biological molecules, but also aids in the design of small molecule ligands to inhibit or alter their activity. In past examples, functionality mapping has been predominantly applied to the location of favorable sites for small functionalized molecules within the interiors of proteins. In principle, a similar strategy can be applied toward identification of the optimal placement of a functional group on the exterior portion of a molecule or molecular assembly. As part of our program to develop computational methods for the design of chiral auxiliaries and catalysts,[3] we have investigated the utility of functionality mapping in this context. Application of functionality mapping to the transition structure of an organic reaction would permit identification of the optimal interactions between defined functional groups and the transition structure.[4] Knowledge of these interactions

* Address for correspondence to this author. Telephone: (215) 898-3048. Fax: (215) 573-7165.

(1) (a) Miranker, A.; Karplus, M. *Proteins: Struct. Funct. Genet.* **1991**, *11*, 29. (b) For a related study see: Hart, T. N.; Read, R. J. *Proteins: Struct. Funct. Genet.* **1992**, *13*, 206.

(2) (a) Caflisch, A.; Miranker, A.; Karplus, M. *J. Med. Chem.* **1993**, *36*, 2142. (b) Zheng, Q.; Kyle, D. J. *Proteins: Struct. Funct. Genet.* **1994**, *19*, 29324. (c) Ringe, D. *Curr. Opin. Struct. Biol.* **1995**, *5*, 825. (d) Ringe, D. *Protein Eng.* **1995**, *8*, 111. (e) Mattos C.; Ringe D. *Nat. Biotechnol.* **1996**, *14*, 595. (f) Sezerman, U.; Vajda, S.; DeLisi, C. *Protein Sci.* **1996**, *5*, 1272. (g) Laskowski, R. A.; Thornton, J. M.; Humblet, C.; Singh, J. *J. Mol. Biol.* **1996**, *259*, 175. (h) Allen, K. N.; Bellamacina, C. R.; Ding, X. C.; Jeffery, C. J.; Mattos, C.; Petsko, G. A.; Ringe, D. *J. Phy. Chem.* **1996**, *100*, 2605. (i) Caflisch A. *J. Comput.-Aided Mol. Des.* **1996**, *10*, 372. (j) Grootenhuis, P. D. J.; Karplus, M. *J. Comput.-Aided Mol. Des.* **1996**, *10*, 1. (k) Joseph-McCarthy, D.; Fedorov, A. A.; Almo, S. C. *Protein Eng.* **1996**, *9*, 773. (l) Joseph-McCarthy, D.; Hogle, J. M.; Karplus, M. *Proteins* **1997**, *29*, 32. (m) Caflisch, A.; Walchli, R.; Ehrhardt, C. *News Phys. Sci.* **1998**, *13*, 182. (n) Leclerc, F.; Karplus, M. *Theor. Chem. Acc.* **1999**, *101*, 131. (o) Castro, A.; Richards, W. G.; Lyne P. D. *Med. Chem. Res.* **1999**, *9*, 98. (p) Stultz, C. M.; Karplus, M. *Proteins* **1999**, *37*, 512. (q) English, A. C.; Groom, C. R.; Hubbard R. E. *Protein Eng.* **2001**, *14*, 47. (r) Ahmed, S.; Majeux, N.; Caflisch A. *J. Mol. Graphics Modell.* **2001**, *19*, 307. (s) Joseph-McCarthy, D.; Tsang, S. K.; Filman, D. J.; Hogle, J. M.; Karplus, M. *J. Am. Chem. Soc.* **2001**, *123*, 12758.

10.1021/jo020401s CCC: $25.00 © 2003 American Chemical Society
Published on Web 09/11/2002

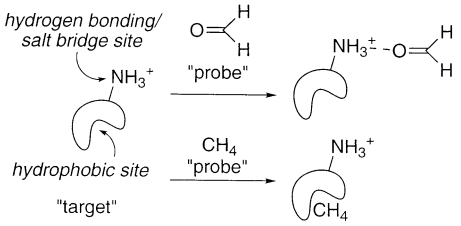

FIGURE 1. Schematic of the functionality mapping program.

could then be used in the construction of ligands and catalysts to stabilize one transition structure, and hence favor one reaction pathway with respect to others.

For ligand-promoted asymmetric organic reactions, studying functional group interactions in the transition states[5] could aid in the generation of new ligands with better selectivity/activity. In this paper we propose a method based on energy minimization for determining the energetically favorable positions of functional groups with respect to the transition states of stereoselective reactions mediated by chiral ligands.

Computational Methods

The functionality mapping calculations involve sequential independent energy minimization of a series of the same functional group (called "probes") placed randomly around the interacting structure (called the "target") with use of the FUNGEN program.[6] MacroModel[7] was used for the generation and visualization of the input and output structures. The CAVEAT CLASS[8] program was used to cluster and order the output. The final result of this process is a set of functional group placements which are sorted by the calculated interaction energy between the target and the probe. The identification of a small number of energetically favorable probe positions from a large number of initial probes indicates that the space around the target has been thoroughly examined and that only a few functional group placements are optimal. When overlapped with the target molecule, each of these functional group placements indicates a possible favorable binding location for that functional group (Figure 1). The net result is a mapping of the portions of the structure with which the functional group interacts favorably.

The target can be a portion of a large system for which information is desired or it can be a whole molecule. We have taken the modeled transition states (without chiral auxiliaries) of boron aldol, boron allylation, and iminium Diels–Alder reactions as our targets in an effort to determine favorable locations and orientations of groups for incorporation into a ligand to control the reaction enantioselectivity. The target transition structures were generated by using a modified MM2* force field[9] for the boron aldol and boron allylation reaction.[10] For the iminium Diels–Alder reaction, targets were obtained from both MM2*[11] and HF/3-21G transition structures.[12] During the functionality mapping, the target transition state was held fixed (rigid body minimization). This feature was useful in that more accurate HF/3-21G transition state geometries[13] could be used.

Once the targets (transition states) for the functionality mapping were generated, the first step of the process was to generate a set of surface points around the target.[14] During initial placement of functional group probes around the target, the user can choose to locate groups around all parts of the target or around select portions. The latter feature is useful if the user does not wish functional groups to be found for certain locations (i.e., too far away from a chiral auxiliary or catalyst attachment point). In this work, the entire surface of the transition state was studied to obtain a complete picture of the most favorable interactions sites. The sampling method places a probe perpendicular to a random point on the surface of the target at a random distance and orientation within a user-defined range. These probes are

(3) Papers in this series: (a) Kozlowski, M. C.; Panda, M. Computer-Aided Design of Chiral Ligands. Part I. Database Search Methods to Identify Chiral Ligand Types for Asymmetric Reactions. In *J. Mol. Graphics Modell.* **2002**, *20*, 399–409. (b) Kozlowski, M. C.; Evans, Catherine A. Computer-Aided Design of Chiral Ligands. Part III. Novel Auxiliaries for Selective Boron Aldol and Allylation Reactions. In preparation.

(4) For recent work on transition state placement in antibody binding sites, see: Tantillo, D. J.; Houk, K. N. *J. Comput. Chem.* **2002**, *23*, 84.

(5) For cases in which the relative energies of the diastereomeric transition states incorporating the chiral ligands correlate to the experimentally measured product selectivity.

(6) *FUNMAP*; G. Lauri, developed in the laboratory of Paul A. Bartlett, U. C. Berkeley. This program uses the same prinicples as the MCSS method of Miranker and Karplus (ref 1). FUNMAP was benchmarked by using the cases studied in ref 1a and was found to perform similarly.

(7) (a) *MacroModel* V4.0, V5.0, V6.0, V6.5; Still, W. C.; Columbia University. (b) Mohamdi, F.; Richards, N. G.; Guida, W. C.; Liskamp, R.; Lipton, M.; Caufield, C.; Chang, G.; Hendrickson, T.; Still, W. C. *J. Comput. Chem.* **1990**, *11*, 440.

(8) (a) Lauri, G.; Bartlett, P. A. *J. Comput.-Aided Mol. Des.* **1993**, *8*, 51. (b) *CAVEAT* V2.2; Bartlett, P. A.; U. C. Berkeley.

(9) Aldol force field: (a) Bernardi, A.; Capelli, A. M.; Gennari, C. *J. Org. Chem.* **1990**, *55*, 3576. (b) Bernardi, A.; Capelli, A. M.; Comotti, A.; Gennari, C.; Gardner, M.; Goodman, J. M.; Paterson, I. *Tetrahedron* **1991**, *47*, 3471. (c) Bernardi, A.; Cassinari, A.; Comotti, A.; Gardner, M.; Gennari, C.; Goodman, J. M.; Paterson, I. *Tetrahedron* **1992**, *48*, 4183. (d) Gennari, C.; Vieth, S.; Comotti, A.; Vulpetti, A.; Goodman, J. M.; Paterson, I. *Tetrahedron* **1992**, *48*, 4439. (e) Vulpetti, A.; Bernardi, A.; Gennari, C.; Goodman, J. M.; Paterson, I. *Tetrahedron* **1993**, *49*, 685. Allylation force field: (f) Vulpetti, A.; Gardner, M.; Gennari, C.; Bernardi, A.; Goodman, J. M.; Paterson, I. *J. Org. Chem.* **1993**, *58*, 1711.

(10) For a further description of these transition states and for a discussion of stereodiscriminating groups, see ref 3a.

(11) The Diels–Alder transition state parameters included in MacroModel 6.5 were used to obtain the MM2* transition states. See Supporting Information.

(12) Panda, M.; Kozlowski, M. C. Unpublished results. HF/3-21G transition states were located with Gaussian98: Frisch, M. J.; Trucks, G. W.; Schlegel, H. B.; Scuseria, G. E.; Robb, M. A.; Cheeseman, J. R.; Zakrzewski, V. G.; Montgomery, J. A., Jr.; Stratmann, R. E.; Burant, J. C.; Dapprich, S.; Millam, J. M.; Daniels, A. D.; Kudin, K. N.; Strain, M. C.; Farkas, O.; Tomasi, J.; Barone, V.; Cossi, M.; Cammi, R.; Mennucci, B.; Pomelli, C.; Adamo, C.; Clifford, S.; Ochterski, J.; Petersson, G. A.; Ayala, P. Y.; Cui, Q.; Morokuma, K.; Malick, D. K.; Rabuck, A. D.; Raghavachari, K.; Foresman, J. B.; Cioslowski, J.; Ortiz, J. V.; Stefanov, J. V.; Liu, G.; Liashenko, A.; Piskorz, P.; Komaromi, I.; Gomperts, R.; Martin, R. L.; Fox, D. J.; Keith, T.; Al-Laham, M. A.; Peng, C. Y.; Nanayakkara, A.; Gonzalez, C.; Challacombe, M.; Gill, P. M. W.; Johnson, B.; Chen, W.; Wong, M. W.; Andres, J. L.; Gonzalez, C.; Head-Gordon, M.; Replogle, E. S.; Pople, J. A. *Gaussian 98*, Revision A.6; Gaussian, Inc.: Pittsburgh, PA, 1998.

(13) Charges for the HF/3-21G transitions states were obtained by single point calculations in MacroModel. The charge distribution was not found to significantly alter the results for the cases in this paper, but more accurate charges may be needed with other probes and targets.

(14) Surface points were generated with the MS program of Connolly: (a) Connolly, M. L. *J. Mol. Graphics* **1993**, *11*, 139. (b) The molecular surface program (MS) was obtained separately from the Quantum Chemistry Program Exchange (QCPE No. 429; http://qcpe.chem.indiana.edu).

then filtered to eliminate initial positions that result in van der Waals overlap or that are too remote from the surface.

After initial placement, the probes are minimized. In this case, the MM2* force field was used to minimize the filtered probes with respect to the rigid body target.[15] The substructure minimization in MacroModel is very fast (2−5 s per probe depending on probe, target, and convergence criteria), so that a mapping run could be completed quite rapidly.[16] Since only the nonbonded parameters incorporated in MM2* are responsible for driving the probes to minimized locations around the target, van der Waals forces and electrostatics are the only interactions considered between the probe and the target. More sophisticated $\pi-\pi$ and CH$-\pi$ interactions are not explicitly incorporated but are approximated to some extent by the van der Waals parameters. The output is a series of probes located near the target which possess negative interaction energies (probes which drift away from the target have interaction energies of zero).

After this minimization, the CAVEAT CLASS[8] program sorts and groups the output probes. Heavy atom number matching is used to compare the output probes and probes that converge to the same point within a user-defined RMSD are grouped into clusters. Symmetry is not taken into account in this comparison. As such, symmetric probes give rise to several clusters with identical positions. For example, benzene is D_{6h} and 6 identical clusters are possible at each position. Overall, the higher the ratio of the starting number of probes to the number of resultant clusters, the more likely that the space around the target has been fully mapped. For example, in the work described below 100−200 starting probes are typically used, which result in 10−50 clusters. For the case with only 10 clusters, it is fairly likely that the most favorable interaction sites have been found. For the case with 50 clusters, additional favorable sites may be possible and can be found by using a larger number of initial probes. The clusters are sorted by energy and a representative probe is written to an output file for each cluster.

The FUNMAP[6] program incorporates the FUNGEN and CLASS modules and automates the entire process going from a target and probe input to cluster locations, so a set of targets and standard probes can be fully evaluated consistently and routinely.

Results and Discussion

The purpose of this study is to determine if the functionality mapping protocol provides a realistic and usable assessment of the optimal positions of a given functional group with respect to a transition state structure. As part of this effort, the ability of functionality mapping to reproduce the positions of the stereodiscriminating fragments[10] of highly selective known ligands was investigated. To accomplish this goal, the parameters of the functionality mapping, the characteristics of the target transitions states, and the features of the probe structures necessary to obtain usable results have been optimized. In the following sections, results from functionality mapping of boron aldol, boron allylation, and iminium Diels−Alder transition states are presented. The insights that the functional group maps offer into stabilizing selected reaction pathways are discussed.

Aldol Reactions. Stereochemical control of the aldol reaction with unsubstituted alkene derivatives involves the selective formation of one enantiomer via control of facial (*re* vs *si*) approach to a prochiral aldehyde (eq 1).

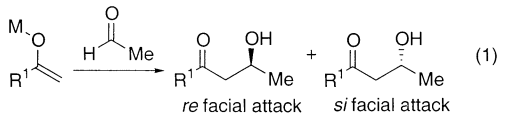

(1)

For substituted alkene derivatives, control of the facial approach with respect to the alkene is also required to set a second stereocenter and achieve a diastereoselective reaction. Numerous auxiliaries and catalysts have been developed such that many aldol reactions can be performed with a remarkable degree of selectivity.[17] These reactions have also been examined extensively experimentally and theoretically.[18,19]

From these studies, a high degree of mechanistic understanding has been achieved.[3a,9a−e,18] For the boron variants, the absence of turnover and any elements past the second row of the periodic table greatly simplifies any computational analysis. Using a force field developed for molecular mechanics calculations of boron aldol[9a−e] transition states, Gennari et al. have designed a new chiral ligand that is selective in this reaction.[20] This achievement demonstrates that force field calculations can provide enough discrimination to aid in the development of new chiral ligands.[21] For these reasons, we selected the boron aldol reaction for our first functionality mapping study and examined the three chiral auxiliaries illustrated in Figure 2. In these reactions, chiral boron enolates are generated and then added to achiral aldehydes. Primarily one diastereomeric product is formed

(15) Parameters need to be specified for FUNMAP to determine which portions of the target are used for the minimization and/or allowed to move during the minimization of the probes. In this case, the entire target structure was utilized in generating the nonbonded interactions with the probes and the target structure was held fixed.

(16) The CPU time required to run the FUNMAP program on an SGI Octane (R10,000) with 100 probes and the transition states described in the text ranged from 1 min to 2 h. See Supporting Information.

(17) (a) Nogradi, M. *Stereoselective Synthesis: A Practical Approach*, 2nd ed.; VCH: Weinheim, Germany, 1995. (b) *Comprehensive Asymmetric Catalysis*; Jacobsen, E. N., Pfaltz, A., Yamamoto, H., Eds.; Springer-Verlag: Berlin, Germany, 1999; Vols. I−III.

(18) For lead references: *Comprehensive Organic Synthesis*; Trost, B. M., Fleming, I., Eds.; Pergamon Press: Oxford, UK, 1991; Vol. 2 (Heathcock, C. H., Volume Ed.).

(19) (a) Li, Y.; Paddon-Row, M. N.; Houk, K. N. *J. Am. Chem. Soc.* **1988**, *110*, 3684. (b) Li, Y.; Paddon-Row, M. N.; Houk, K. N. *J. Org. Chem.* **1990**, *55*, 481 and references therein. (c) Bernardi, F.; Robb, M. A.; Suzi-Valli, G.; Tagliavini, E.; Tromboni, C.; Umani-Ronchi, A. *J. Org. Chem.* **1991**, *56*, 6472.

(20) For the design of the dimenthylborane aldol chiral auxiliary see: (a) Gennari, C.; Hewkin, C. T.; Molinari, F.; Bernardi, A.; Comotti, A.; Goodman, J. M.; Paterson, I. *J. Org. Chem.* **1992**, *57*, 5173. (b) Paterson, I. *Pure Appl. Chem.* **1992**, *64*, 1821. (c) Gennari, C.; Moresca, D.; Vieth, S.; Vulpetti, A. *Angew. Chem., Int. Ed. Engl.* **1993**, *32*, 1618. (d) Bernardi, A.; Comotti, A.; Gennari, C.; Hwekin, C. T.; Goodman, J. M.; Schlapbach, A.; Paterson, I. *Tetrahedron* **1994**, *50*, 1227. (e) Bernardi, A.; Gennari, C.; Goodman, J. M.; Paterson, I. *Tetrahedron: Asymmetry* **1995**, *6*, 2613. (f) Gennari, C. *Pure Appl. Chem.* **1997**, *69*, 507. (g) Gennari, C.; Ceccarelli, S.; Piarulli, U.; Aboutayab, K. *J. Braz. Chem. Soc.* **1998**, *9*, 319.

(21) For examples in other systems see: *Transition State Modeling for Catalysis*; ACS Symp. Ser. No. 721: Truhlar, D. G., Morokuma, K., Eds.; American Chemical Society: Washington, DC, 1999; and references contained therein.

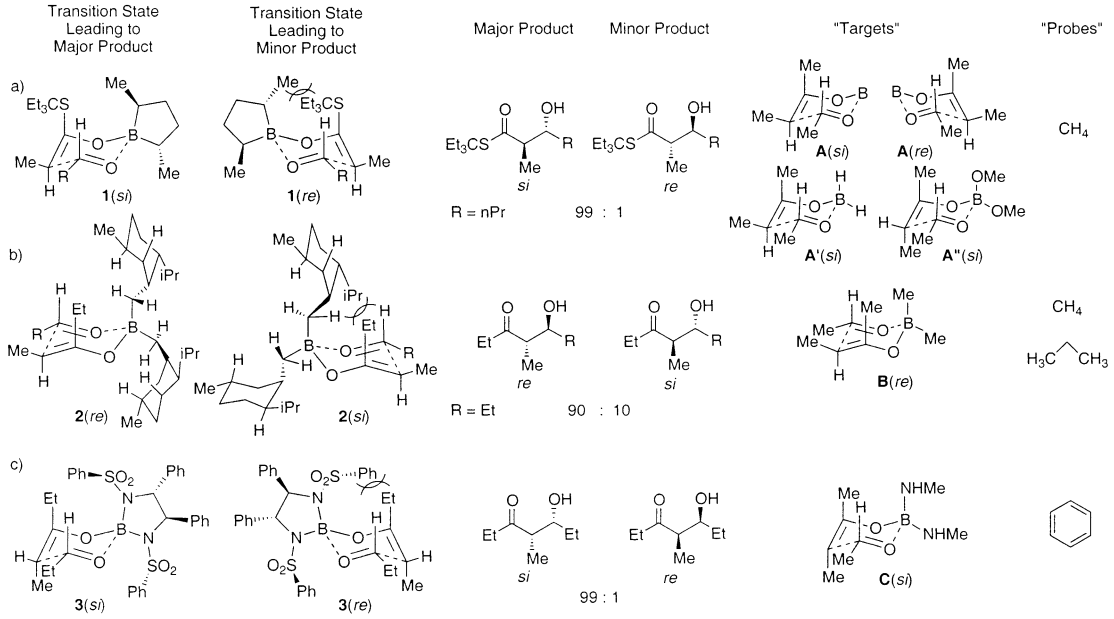

FIGURE 2. Boron aldol transition states and products along with the corresponding targets and the probes used for the functionality mapping program: (a) Masamune dimethylborolane, (b) dimenthylborane, and (c) Corey stien reagent.

as a mixture of enantiomers. The proposed transition structures leading to these enantiomers as well as the enantiomeric ratios are collected in Figure 2.

In the first example, the boron aldol reaction promoted by the Masamune dimethylborolane[22] was analyzed. In Figure 2a, the transition states **1**(*si*) and **1**(*re*) leading to the major and minor products, respectively, are illustrated. Analysis of these structures[22,23] suggests that the methyl groups attached to the carbon atom of the ligand adjacent to the boron are the stereodiscriminating groups.[10] To determine the most favorable locations of functional groups, the chiral ligand was excised from the lowest energy transition state and the new structure was minimized[24] providing core transition structure **A′**(*si*). Hydrogens were used as stand-in substituents for the ligand on the boron. If substituents larger than hydrogen, such as methyl groups, were employed, functional groups were not mapped to some favorable locations due to steric interactions with these substituents. For example, methane clusters were not found corresponding to the positions of the methyl stereodiscriminating groups in the Masamune dimethylborolane when $B(Me)_2$ is used but were found when $B(H)_2$ is used. Use of divalent boron transition state **A**(*si*) with no substituents corresponding to the ligand also alleviated this problem.

Next, a series of functional group probes were minimized with respect to the transition state **A**(*si*). In this case, the methane probe was selected to stand in for the stereodiscriminating methyl substituents of the Masamune dimethylborolane chiral auxiliary. Thus, a series of methane molecules were randomly placed around the surface of chair transition state **A**(*si*). These methanes were then minimized to the surface of the transition state independently of one another. The results of these minimizations were found to be only weakly dependent upon the gradient method used to find minima along the potential energy surface (Table 1). In all cases, a cluster of methane probes was found near one of the stereodiscriminating groups of the Masamune dimethylborolane (see below), indicating that this interaction can be reproduced regardless of the gradient. With the TNCG and PRCG gradients a smaller number of clusters was found and all the clusters possessed good interaction energies.[25]

The nonpolar nature of the methane molecule leads to a weak interaction (−5 to −8 kJ/mol) with the target. As such, the methane molecules were found to distribute over large portions of the surface of the model transition state; however, discrete clusters did form. When starting

TABLE 1. Relationship between the Starting Number of Methane Probes and the Output Clusters Found with the PRCG and TNCG Gradients in the Functionality Mapping of A

					population of clusters				
entry	TS	gradient[a]	no. of probes	no. of clusters[b]	1st	2nd	3rd	4th	5th
1	**A**(*si*)	PRCG	200	10	29	43	33	26	13
2[c]	**A**(*si*)	PRCG	200	10	32	24	34	31	26
3	**A**(*si*)	PRCG	500	11	81	91	75	73	61
4	**A**(*si*)	PRCG	1000	12	148	196	189	147	119
5	**A**(*re*)	PRCG	200	10	33	31	45	30	28
6	**A**(*re*)	PRCG	500	10	74	89	88	77	72
7	**A**(*si*)	TNCG	200	9	23	47	37	25	25
8[c]	**A**(*si*)	TNCG	200	9	22	40	49	25	29
9	**A**(*si*)	TNCG	500	9	89	82	91	72	62
10	**A**(*si*)	TNCG	1000	9	168	181	188	151	120
11	**A**(*re*)	TNCG	200	9	43	25	28	39	29
12	**A**(*re*)	TNCG	500	9	90	99	89	66	58

[a] Convergence criteria: PRCG 0.001 kJ/(mol·Å); TNCG 0.01 kJ/(mol·Å). [b] A 1.0 Å RMSD (heavy atoms) was used for clustering. [c] Repeat of the run in the prior table entry.

(22) (a) Masamune, S.; Sata, T.; Kim, B. M.; Wollmann, T. A. *J. Am. Chem. Soc.* **1986**, *108*, 8279. (b) For the related diphenylborolane in aldol reactions see: Reetz, M. T.; Heitmann, P. *Tetrahedron Lett.* **1986**, *27*, 4721.

(23) For an example of the correlation of the reaction selectivity with calculated transition state energies for the Masamune dimethylborolane see ref 9c.

(24) Very little change in the geometry of the core portion of the transition state occurred upon minimization, indicating that the ligand induces very little strain into this structure.

TABLE 2. Functionality Mapping Results for the Aldol Transition States in Figure 2[a]

entry	target	relevant TS[b]	probe	no. of clusters[c]	populations; energies (kJ/mol) of the top five clusters 1st	2nd	3rd	4th	5th	energy range (kJ/mol)	distance in Å (energy in kJ/mol, cluster no.)[d]
1	**A**(*si*)	**1**(*si*)	CH_4	9	23; 7.84	47; −7.78	37; −7.26	25; −7.09	25; −7.05	−7.84 to −5.19	0.95 (−7.05, 5) 3.11 (−7.78, 2)
2	**A**(*re*)	**1**(*re*)	CH_4	9	28; −7.84	31; −7.78	47; −7.26	32; −7.09	25; −7.05	−7.84 to −5.19	1.80 (−7.05, 5) 2.58 (−7.78, 2)
3	**A′**(*si*)	**1**(*si*)	CH_4	9	28; −8.50	35; −7.92	34; −7.31	23; −7.13	11; −7.13	−8.50 to −5.81	1.66 (−7.13, 4) 2.59 (−8.50, 1)
4	**A″**(*si*)		CH_4	8	39; −10.88	29; −10.51	38; −9.45	8; −9.21	20; −8.99	−10.88 to −6.97	
5	**A″**(*re*)		CH_4	8	38; −9.82	41; −9.61	33; −9.63	20; −9.52	29; −9.47	−9.82 to −6.92	
6	**B**(*re*)	**2**(*si*)	CH_4	15	19; −9.34	12; −8.68	11; −8.53	10; −8.32	19; −8.30	−9.344 to −3.9	Me: 1.29 (−8.53, 3) Me: 2.12 (−8.30, 5) ^{i}Pr: 0.84 (−3.94, 16) ^{i}Pr: 3.45 (−7.01, 11)
7	**B**(*re*)	**2**(*si*)	propane	106	2; −15.48	2; −15.14	3; −14.93	1; −14.85	1; −14.80	−15.48 to −5.79	Me: 0.64 (−14.43, 11) Me: 0.89 (−14.65, 7)
8	**C**(*si*)	**3**(*si*)	PhH	74[e]	9; −21.61	6; −21.61	7; −21.61	5; −21.61	5; −21.61	−21.61 to −11.86	0.90[f] (−19.29, 21) 1.33[f] (−21.61, 1)

[a] 200 probes with a TNCG gradient and a convergence criterion of 0.01 kJ/(mol·Å) were used in all cases. [b] Corresponds to the transition state incorporating the relevant chiral auxiliary (see Figure 2), which is being compared to the target and its functionality map. [c] A 1.0 Å RMSD (heavy atoms) was used for clustering. [d] Distances between stereodiscriminating groups of the transition state from the third column and their closest clusters. The interaction energy of these clusters and their rank, in terms of favorable interaction energy, are given in parentheses. [e] The high symmetry of benzene leads to mapping of up to 6 identical clusters having the same interaction energy. [f] RMSD values comparing the 6 carbons of the benzene probe with those of the phenyl group.

with 200 methane probes using a PRCG gradient, 10 clusters were reproducibly found (Table 1, entries 1 and 2) which were not uniformly distributed but favored impressions in the transition state surface. With larger numbers of probes (500 and 1000, entries 3 and 4), only 1−2 additional weakly interacting clusters were found using the PRCG gradient and the identity of the clusters with the best interaction energies remained unchanged.

With the TNCG gradient, the number of resultant clusters was found to be reproducible (entries 7 and 8) and constant regardless of the number of starting probes (entries 7−10). For the remainder of the cases described in this paper the TNCG gradient was employed. In all searches, these clusters were found multiple times, indicating that the search method was identifying the most energetically favorable points of occupancy for a methane group around the target transition state. The only difference lay in the population of the clusters as would be expected for a converged random sampling method. The use of a larger number of starting points did not provide further new low-energy clusters in either of these cases, but may be necessary to fully explore all possible positions when the ratio of starting probes to clusters is low. As expected, similar distributions and the same numbers of clusters were found when the enantiomeric targets were employed (entries 5, 6, 11, and 12).

Table 2 lists the functionality mapping results for a number of probes against the targets illustrated in Figure 2. In addition to the number of clusters, the energies of interaction between the probes and transition structures are listed for the five clusters with the most favorable interaction energy. The rank and interaction energy of the cluster that best reproduces the position of "stereodiscriminating groups" found in known chiral auxiliaries is listed in the last column. The details of these results are discussed below as they relate to each target.

Figure 3a illustrates the methane clusters (Table 2, entry 1) along with the **A**(*si*) transition structure (shown as the half-bond line structure) used for the functionality mapping. The methane clusters are colored (red, orange, yellow) according to their interaction energy with the transition state. The reddest clusters have the largest favorable interactions and the most yellow clusters have the smallest favorable interactions. Although the methane probes did distribute over large portions of the transition state surface, the most favorable points of interaction were above and below the plane of the chair transition state as well as near the oxygen heteroatoms of the aldehyde and enolate. Such a result is consistent with an optimization of van der Waals interactions. Shallow depressions above and below the plane of the chair transition state allow for the maximal surface area of interaction with the probes while the more electronegative heteroatoms provide the strongest interactions.

In a second analysis, a similar functionality map (Figure 3b) was constructed from 200 methane molecules with use of the enantiomeric transition state **A**(*re*) (Table 2, entry 2). Here, 9 clusters were identified. Inspection of the functionality maps from enantiomeric transition structures **A**(*si*) and **A**(*re*) reveals that the maps are mirror images of one another, verifying that the functionality mapping is robust and reproducible.

When the methane clusters from **A**(*si*) were overlaid with the lowest energy *si* transition state incorporating the Masamune dimethylborolane ligand [**1**(*si*), corresponds to the major product formed, Figure 2a], we

(25) In contrast, the OSVM, FMNR, and SD gradients effect a more thorough search of the potential energy surface environment and identify shallower minima. This trend is confirmed by the wider range of interaction energies exhibited by the clusters when these gradients were employed (see Supporting Information). Similar trends were also observed for other functional group probes such as benzene, methyl acetate, and methyl formate. In terms of utility, the TNCG and PRCG gradients were found to provide the best compromise between identification of all sites of interaction and identification of the most favorable interaction sites.

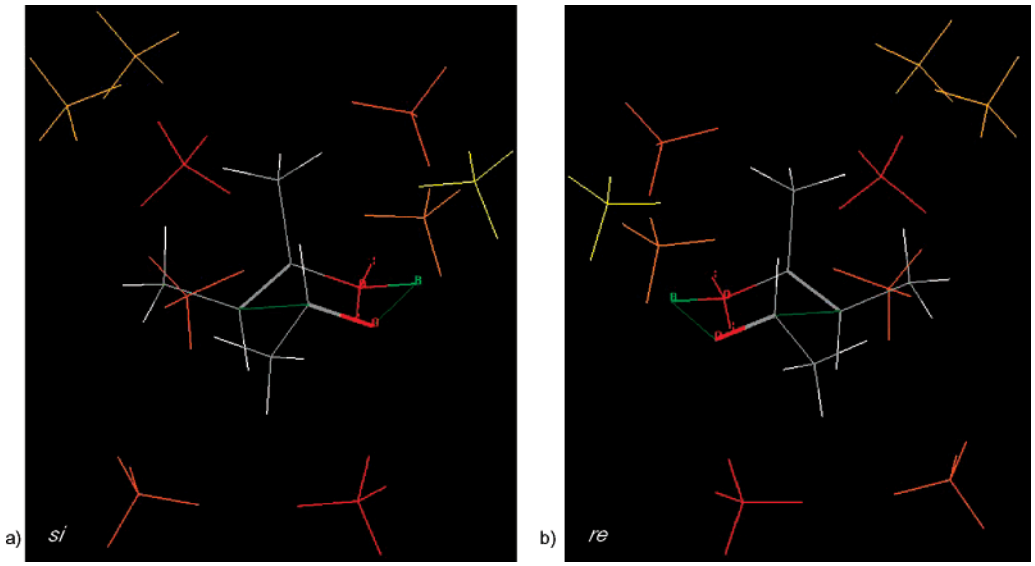

FIGURE 3. Functionality mapping of target **A** with 200 methane probes. The reddest clusters have the largest favorable interactions and the most yellow clusters have the smallest favorable interactions: (a) target **A**(*si*), 9 clusters were found; (b) target **A**(*re*), 9 clusters were found.

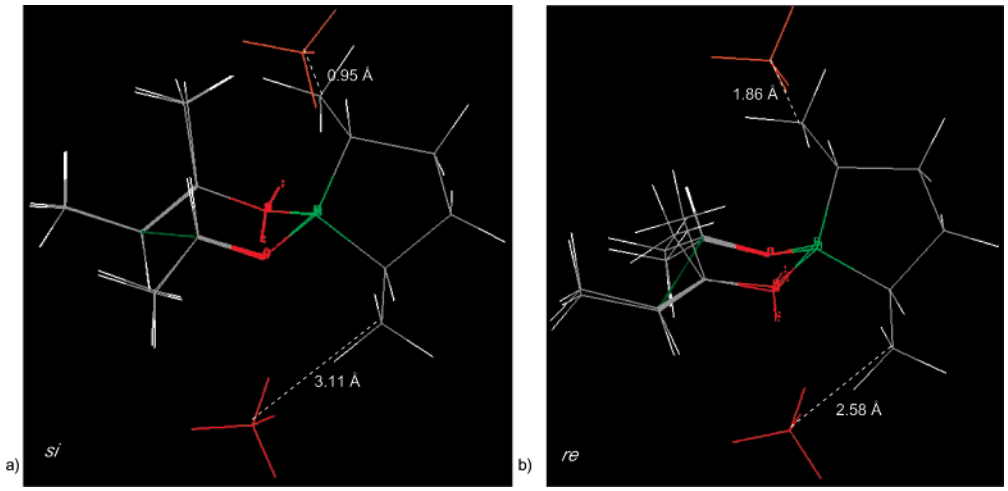

FIGURE 4. Functionality mapping of target **A** with 200 methane probes. The reddest clusters have the largest favorable interactions and the most yellow clusters have the smallest favorable interactions. Only the probes closest to the stereodiscriminating groups of the chiral ligand are illustrated. (a) Target **A**(*si*) is overlaid with **1**(*si*). (b) Target **A**(*re*) is overlaid with **1**(*re*).

observed that a number of the clusters were centered close to the stereodiscriminating methyl groups of the ligand (Figure 4a). In contrast, the overlay of the methane clusters from **A**(*re*) with the lowest energy *re* transition state incorporating the Masamune dimethylborolane ligand [**1**(*re*), corresponds to the minor product formed, Figure 2a] shows a less favorable overlap between the methane clusters and the stereodiscriminating methyl groups of the dimethylborolane ligand (Figure 4b).

In Figure 5, these results are presented in an overlay of **1**(*si*) and **1**(*re*). The methane probes from **A**(*si*) and **A**(*re*) found closest to the methyl substituents of the chiral ligand in **1**(*si*) and **1**(*re*), respectively, are also shown. The methanes from **A**(*si*) are closer to the stereodiscriminating methyl substituents in **1**(*si*) (purple) than the methanes from **A**(*re*) are to the stereodiscriminating methyl substituents in **1**(*re*) (yellow). Such an outcome indicates that at least the "upper" methyl substituent of the dimethylborolane ligand is positioned to incur favorable interactions in the *si* selective process via **1**(*si*) and less favorable interactions in the *re* selective process via **1**(*re*). No good match is found in the functionality mapping for the "lower" methyl substituent of the dimethylborolane ligand, which is consistent with the proposal that this substituent does not markedly stabilize either pathway due to its distal location from the chair cyclic portion of these aldol transition states.[22]

From this analysis a slightly different picture emerges for the source of selectivity in the aldol reactions utilizing the Masamune dimethylborolane (Figure 6). The energy diagram in Figure 6b qualitatively illustrates the analysis described previously[22] wherein the upper methyl substituent of **1**(*re*) destabilizes this diastereomeric pathway. On the other hand, the energy diagram in Figure 6c reflects the results described above wherein the upper methyl substituent destabilizes **1**(*re*) *and stabilizes* **1**(*si*). The concept of steric destabilizing interactions as a means to influence reaction selectivity is well-accepted.

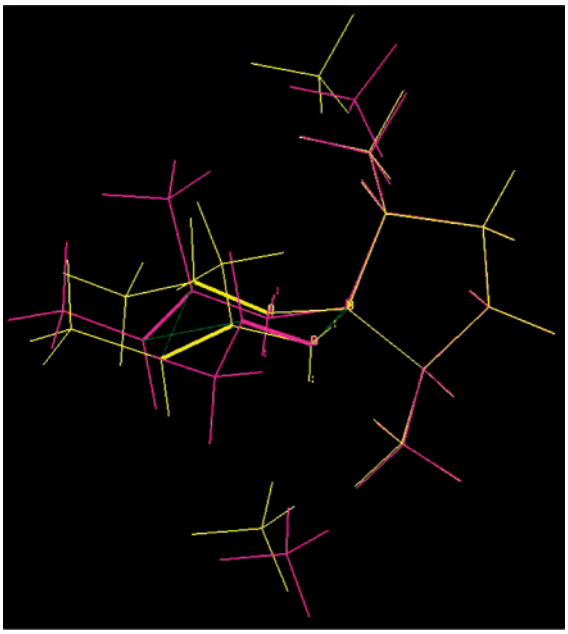

FIGURE 5. Overlay of **1**(*si*) (purple) and **1**(*re*) (yellow). The methane probes from the corresponding functionality maps of **A**(*si*) and **A**(*re*) which are closest to the methyl substituents of the chiral ligands are also shown.

However, there are fewer examples utilizing nonbonded *stabilizing* interactions to influence selectivity. The analyses described herein indicate that the latter mode of discrimination may be more widespread than previously appreciated. The functionality mapping provides a rapid method to assess both stabilizing and destabilizing nonbonded interactions in order to understand the source(s) of stereodiscrimination in asymmetric reactions.

The functionality mapping can also provide an overall spatial map for a given reaction. Figure 7 superimposes the related dimethoxyborane targets **A**″(*si*) and **A**″(*re*) via their best overlap along with their corresponding methane functionality maps (Table 2, entries 4 and 5). Note that only the carbons of the methane groups are illustrated (at 15% of their van der Waals radii) so that individual methanes can be visually discerned. In space-filling models these methanes completely encompass the transition state and there are significant van der Waals contacts. Analysis of Figure 7 quickly divides the space surrounding the enantiomeric transition structures into several categories. In the first type (Type I), neither enantiomeric transition structure undergoes favorable interactions (negative energy) with the probes at these positions. This may be due to an absence of interactions (zero energy) or due to disfavorable interactions (positive energy), such as overlap of the van der Waals radii. In the second type (Type II), both enantiomeric transition structures favor probes at these positions. In the third type (Type III), only one transition structure prefers probes at these positions. Presumably, there is no favorable interaction or an unfavorable interaction with the enantiomeric transition structure. For example, there is overlap with a methyl substituent of **A**″(*re*) at the circled (Type III) position.

At this point it is a straightforward exercise to select methane groups which favor only the reaction pathway of choice. For example, to design a ligand that directs *si* facial attack to the aldehyde, Type III methane groups that complement **A**″(*si*) would be used as a starting point. These methane groups can then be screened further for candidates which disfavor **A**″(*re*) sterically and which are located in proximity to the boron atom. For example, the C_2-symmetrically disposed methyl groups Me^1 and Me^2 (Figure 7) fulfill these criteria.

In a second example, the boron aldol reaction with dimenthylborane was examined (Figure 2b). Gennari et al. have suggested that the stereoselectivity of the dimenthylborane aldol reaction is controlled by the isopropyl substituents of the cyclohexane rings.[20] These workers identified transition states for these reactions and have shown that calculated selectivities can be used to predict the experimental selectivities. Overlays of the lowest energy transition state incorporating the ligand, **2**(*re*), with the methane and propane functionality maps of **B**(*re*) (Figure 2b) show few clusters near the isopropyl group of the ligand. For the methane functionality map (Figure 8), probes that were found in the vicinity of the isopropyl substituents possessed surprisingly poor interaction energies (Table 2, entry 6). On this basis, we do not expect that the isopropyl groups generate *favorable* interactions in the lowest energy transition state leading to the major product. In contrast, a good number of probes with the most favorable interaction energies are centered around the methyl groups attached to the ligand. This result indicates that the positions of these methyl groups may be important, since favorable van der Waals interactions with the transition state can occur.

The functionality map of **B**(*re*) with propane, as a mimic for the isopropyl substituents, was found to be considerably more complex (Table 2, entry 7). A larger number of clusters (106) were found, 40 of which are illustrated in Figure 9. This larger number of clusters compared to the 15 clusters found in the corresponding methane functionality map arises from the larger number

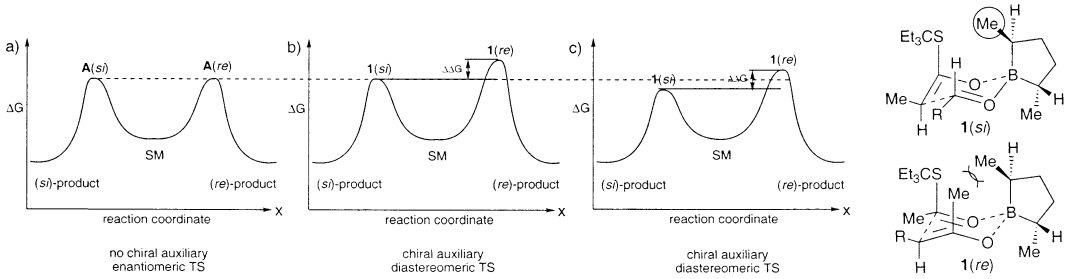

FIGURE 6. Origin of selectivity in the Masamune boron aldol reaction.

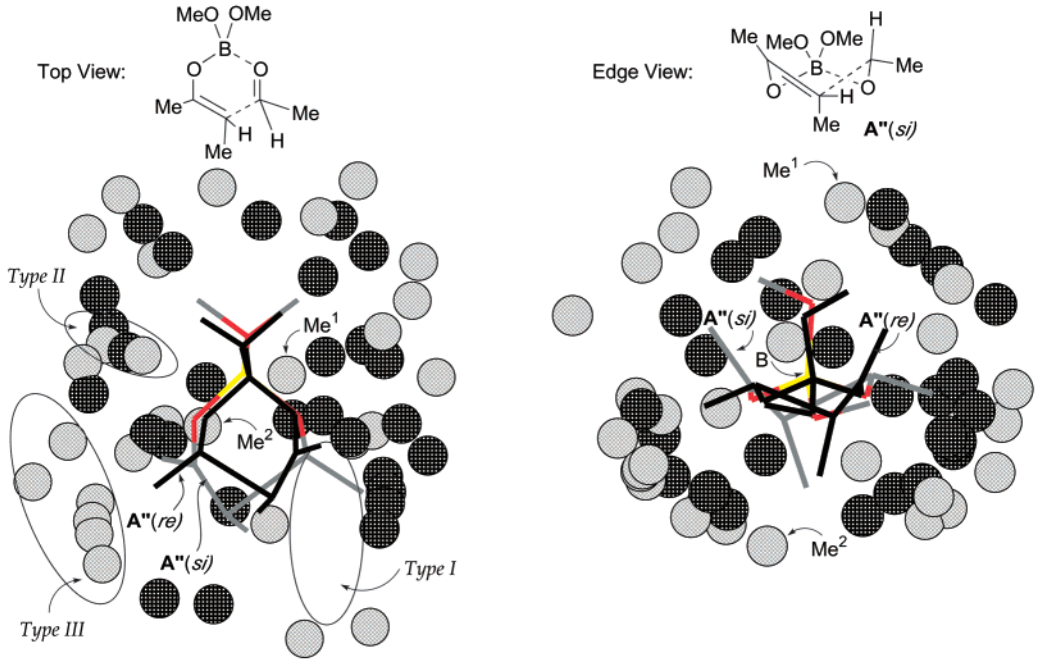

FIGURE 7. Two target transition states **A**″(*si*) and **A**″(*re*) and their accompanying methane functionality maps are overlaid (two orientations shown): **A**″(*si*) = half bond line structure, **A**″(*si*) methanes = light spheres, **A**″(*re*) = solid black line structure, and **A**″(*re*) methanes = dark spheres.

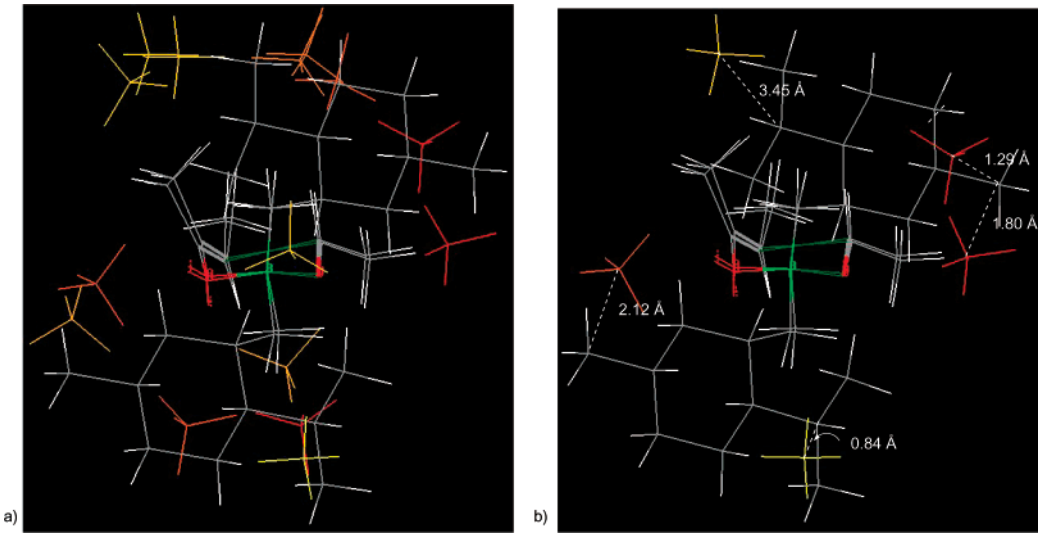

FIGURE 8. Functionality mapping of target **B**(*re*) with methane probes. Target **B**(*re*) is overlaid with **2**(*re*). (a) All clusters found (15) are shown. (b) The clusters closest to the stereodiscriminating group, and the distances between them, are shown.

of conformations available to propane at any single position. The net result is a more complex functionality map. The propane probes predominantly occupy positions near the unsaturated elements of the transition state target compared to the methane probes which distribute over larger portions of the transition state surface. A larger number of energetically favorable positions are available to the methane probes, since these smaller probes are capable of "fitting" into smaller depressions along the transition state surface. The match between the propane probes and the isopropyl substituents in **2**(*re*) is poor (>4 Å), indicating that functionality mapping with *n*-alkyl probes is not effective in this context.

Corey et al. reported several useful ligands based on stilbenediamine (stien)[26] that lead to highly enantioselective boron aldol/allylation adducts (Figure 2c). The orientation of the aryl sulfonyl groups in the chiral ligand was proposed to play a decisive role in the enantioselection. The results from MM2* minimization of the two diastereomeric transition states, **3**(*si*) and **3**(*re*) that lead to the two enantiomeric products, support models put forth by Corey[26] regarding the more stable transition state.[27] For the functionality mapping, transition state **C**(*si*) with B-NHMe as termini was chosen as the target to mimic the boronamidate portion of the stien ligand and benzene was chosen as the probe to mimic the sulfonyl phenyl groups (Figure 2c).

(26) Corey, E. J.; Imwinkelried, R.; Pikul, S.; Xiang, Y. B. *J. Am. Chem. Soc.* **1989**, *111*, 5493.

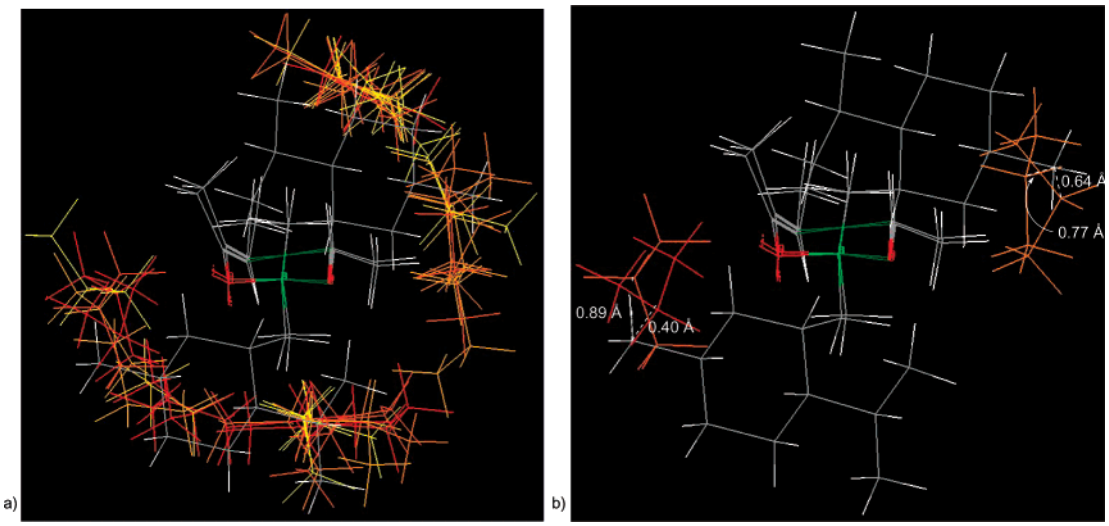

FIGURE 9. Functionality mapping of target **B**(*re*) with propane probes. Target **B**(*re*) is overlaid with **2**(*re*). (a) The first 40 clusters out of the 106 found are shown. (b) The clusters closest to the stereodiscriminating group, and the distances between them, are shown.

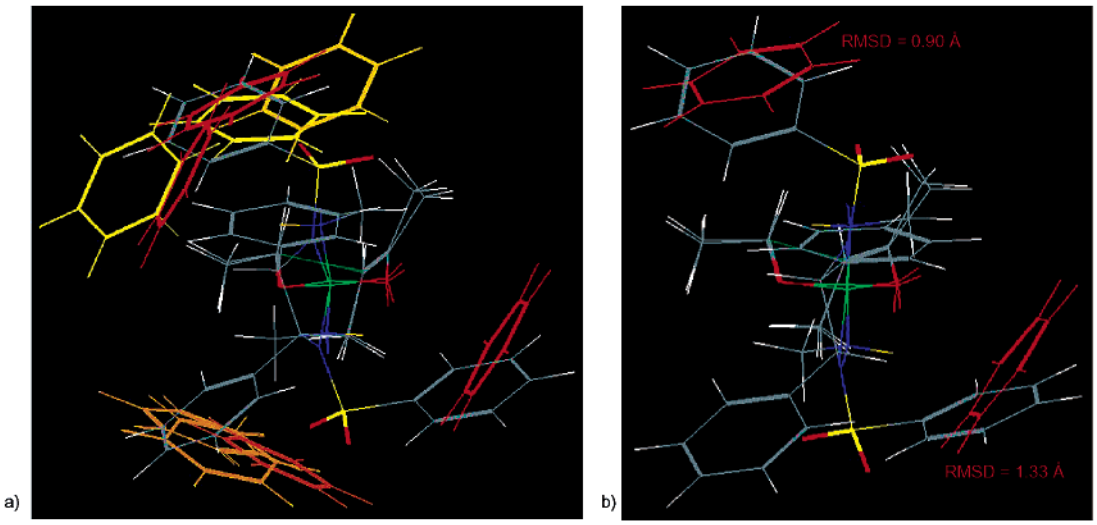

FIGURE 10. Functionality mapping of target **C**(*si*) with benzene probes. Target **C**(*si*) is overlaid with **3**(s*i*). (a) The first 40 clusters out of the 74 found are shown. (b) The clusters closest to the stereodiscriminating phenyl groups, and the RMSD between them, are shown.

The functionality mapping of **C**(*si*) (Table 2, entry 8) revealed three dense populations of probes which were confined to limited regions of the target (Figure 10) unlike the previous functionality maps with methane and propane. This may be due to the relative size of the probe, as benzene is larger than methane. Up to 6 clusters may appear at each particular site of interaction due the high symmetry (D_{6h}) of the benzene. The interactions are stronger than those of methane (−4 to −11 kJ/mol) and range from −12 to −22 kJ/mol (Table 2). When the mapping of target and probes is overlapped with the favored transition state **3**(*si*) suggested by Corey (Figure 2c),[26] the locations of two dense clusters of benzene probes are an excellent match with the phenyl rings of the two arylsulfonyl groups of the C_2-symmetric stien reagent. These benzene clusters also have the most favorable interaction energies with the transition state as indicated by their red or dark orange color in Figure 10. Furthermore, the orientations of the benzene rings are similar to those of the arylsulfonyl phenyl rings. The mapping of the benzene rings on *both sides* of the transition state with little change in interaction energy suggests the importance of both phenyl substituents in the C_2-symmetric ligand in this enantioselective reaction. This result stands in contrast to the dimethylborolane reagent (Figure 2a) in which only one of the methyl substituents appears to be critical (Figure 4).

Allylation Reactions. The use of chiral allyl- and crotylborane reagents has been shown to be valuable for the stereoselective construction of carbon−carbon bonds. The asymmetric allylboration reaction has been studied extensively and enantioselection in this reaction also arises via control of facial (*re* vs *si*) approach to a prochiral aldehyde (eq 2).[28,29,30]

The allylboronates prepared from diisopropyl tartrate (DIPT) react with achiral aldehydes to provide homoallylic alcohols in good yields and high enantioselectivities.[30] The asymmetric induction in these reactions has

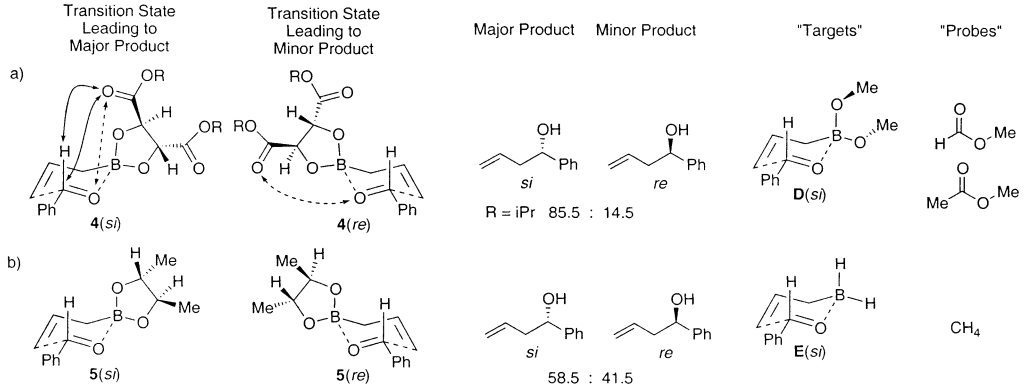

FIGURE 11. Boron allylation transition states along with the corresponding targets and the probes used for the functionality mapping program. Double-head solid arrows indicate stabilizing interactions and double-headed dashed arrows indicate destabilizing interactions.

TABLE 3. Functionality Mapping Results for the Allylboration Transition States in Figure 11[a]

entry	target	relevant TS[b]	probe	no. of clusters[c]	populations; energies (kJ/mol) of the top five clusters 1st	2nd	3rd	4th	5th	energy range (kJ/mol)	distance in Å (energy in kJ/mol, cluster no.)[d]
1	**D**(*si*)	**4**(*si*)	$MeCO_2Me$	66	10; −27.37	31; −26.20	2; −24.42	2; −24.03	6; −23.37	−27.37 to −8.66	2.24 (−27.37, 1) 2.09 (−20.44, 20)
2	**D**(*si*)	**4**(*si*)	HCO_2Me	57	20; −23.34	8; −23.02	10; −21.40	15; −20.68	2 −20.64	−23.34 to 8.60	1.77 (−23.34, 1) 1.96 (−17.48, 16)
3	**E**(*si*)	**5**(*si*)	CH_4	12	46; −9.40	22; −8.75	8; −8.73	6; −7.67	45; −7.66	−9.40 to −4.89	2.75 (−5.93, 9) 4.36 (−4.89, 12)
4	**E**(*re*)	**5**(*re*)	CH_4	12	47; −9.41	15; −8.79	15; −8.78	5; −7.67	47; −7.64	−9.41 to −4.89	1.41 (−5.94, 9) 3.69 (−4.90, 11)

[a] 200 probes with a TNCG gradient and a convergence criterion of 0.01 kJ/(mol·Å) were used in all cases. [b] Corresponds to the transition state incorporating the relevant chiral auxiliary (see Figure 11) which is being compared to the target and its functionality map. [c] A 1.0 Å RMSD (heavy atoms) was used for clustering. [d] Distances between stereodiscriminating groups of the transition state from the third column and their closest clusters. The interaction energy of these clusters and their rank, in terms of favorable interaction energy are given in parentheses.

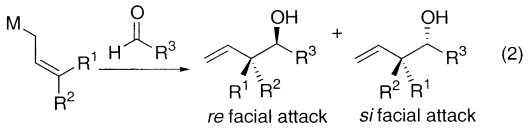

(2)

been ascribed to long-range electronic interactions. Favorable dipole−dipole interactions between the aldehyde carbonyl and the proximate ester stabilize the transition state leading to the major enantiomer and lone pair repulsive interactions between the aldehyde oxygen atom and an ester carbonyl destabilize the transition state leading to the minor enantiomer (Figure 11a).[31,32] Since transition state energy calculations for the addition of (+)-DIPT allyl- and crotylboronates to aldehydes correlate well with experimentally measured selectivities,[33] it appears that these electronic interactions can also be effectively modeled. To determine if functionality mapping could assess advantageous and disadvantageous electronic interactions, the reactions of allylboronates were examined in this context.

The dimethyl borate transition state **D**(*si*) was chosen as the target for the study of the interaction of ester moieties by means of functionality mapping (Table 3, entries 1 and 2). Methoxy groups were retained on the

(27) The two diastereomeric transition states **3**(*si*) and **3**(*re*) (Figure 2c) were minimized by using molecular mechanics (see Supporting Information). The energy difference calculated from the minimized structures corresponds to an 83:17 product ratio. These results compare favorably to the closely related aldol reaction with propionaldehyde (CH_3CH_2CHO) and diethyl ketone examined experimentally by Corey where a 99:1 ratio was observed (see ref 26).

(28) For a review see ref 17a; pp 162−167.

(29) A number of highly selective reagents for aymmetric allylboration of achiral aldehydes have been reported. (a) Hoffmann, R. W.; Herold, T. *Chem. Ber.* **1981**, *114*, 375. (b) Hoffmann, R. W.; Helbig, W. *Chem. Ber.* **1981**, *114*, 2802. (c) Hoffmann, R. W.; Zeiss, H. J.; Ladner, W.; Tabche, S. *Chem. Ber.* **1982**, *115*, 2357. (d) Reetz, M. T.; Zierke, T. *Chem. Ind. (Britain)* **1988**, *20*, 663. (e) Corey, E. J.; Yu, C.-M.; Kim, S. S. *J. Am. Chem. Soc.* **1989**, *111*, 5495. (f) Jadhav, P. K.; Bhat, K. S.; Perumal, P. T.; Brown, H. C. *J. Org. Chem.* **1986**, *51*, 432. (g) Brown, H. C.; Bhat, K. S. *J. Am. Chem. Soc.* **1986**, *108*, 5919. (h) Brown, H. C.; Jadhav, P. K.; Bhat, K. S. *J. Am. Chem. Soc.* **1988**, *110*, 1538. (i) Brown, H. C.; Jadhav, P. K.; Bhat, K. S. *J. Am. Chem. Soc.* **1988**, *110*, 1535. (j) Brown, H. C.; Ramachandran, P. V. *Pure Appl. Chem.* **1991**, *63*, 307. (k) Garcia, J.; Kim, B. M.; Masamune, S. *J. Org. Chem.* **1987**, *52*, 4831. (l) Short, R. P.; Masamune, S. *J. Am. Chem. Soc.* **1989**, *111*, 1892. See also ref 18.

(30) (a) Roush, W. R.; Walts, A. E.; Hoong, L. K. *J. Am. Chem. Soc.* **1985**, *107*, 8186. (b) Roush, W. R.; Banfi, L. *J. Am. Chem. Soc.* **1988**, *110*, 3979. (c) Roush, W. R.; Hoong, L. K.; Palmer, M. A. J.; Park, J. C. *J. Org. Chem.* **1990**, *55*, 4109. (d) Roush, W. R.; Hoong, L. K.; Palmer, M. A. J.; Straub, J. A.; Palkowitz, A. D. *J. Org. Chem.* **1990**, *55*, 4117. (e) Roush, W. R.; Ando, K.; Powers, D. B.; Palkowitz, A.; Halterman, R. L. *J. Am. Chem. Soc.* **1990**, *112*, 6339.

(31) Roush, W. R.; Ratz, A. M.; Jablonowski, J. A. *J. Org. Chem.* **1992**, *57*, 2047.

(32) Using these models, Roush et al. have designed improved chiral auxiliaries: (a) Roush, W. R.; Banfi, L. *J. Am. Chem. Soc.* **1988**, *110*, 3979. (b) Roush, W. R.; Grover, P. T. *J. Org. Chem.* **1995**, *60*, 3806.

(33) We have calculated the transition states for the addition of (+)-DIPT allyl- and crotyl boronates to CH_3CHO and PhCHO, as well as for the addition of the (−)-2,3-butanediol allylboronate to PhCHO. The product ratios calculated from the transition state energies qualitatively agree with the experimentally measured selectivities: Kozlowski, M. C.; Ganguly, B.; Panda, M.; Skudlarek, J. W. *Tetrahedron*. Submitted for publication.

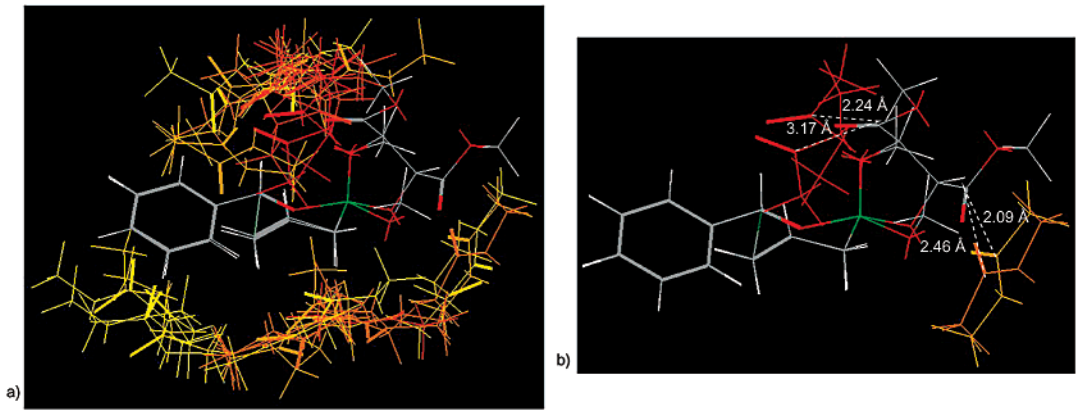

FIGURE 12. Functionality mapping of target **D**(*si*) with methyl acetate probes. Target **D**(*si*) is overlaid with **4**(*si*). (a) The first 40 clusters out of the 66 found are shown. (b) The clusters closest to the stereodiscriminating carbonyl groups, and the distances between the carbonyl carbons, are shown.

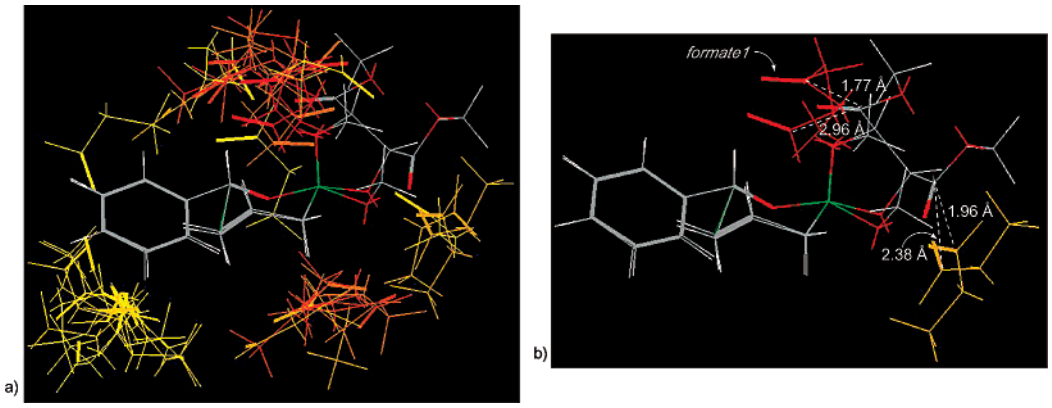

FIGURE 13. Functionality mapping of target **D**(*si*) with methyl formate probes. Target **D**(*si*) is overlaid with **4**(*si*). (a) The first 40 clusters out of the 57 found are shown. (b) The clusters closest to the stereodiscriminating carbonyl groups, and the distances between the carbonyl carbons, are shown.

boron in **D**(*si*) in order to simulate the electrostatic potential and steric size found in the boronate ligand series. Mappings with methyl ester (Figure 12) and formyl ester (Figure 13) probes yielded similar results, although methyl formate is a better probe than methyl acetate. The interaction energies ranged from −27 to −9 kJ/mol, indicating that the probes were undergoing quite strong interactions with the transition state target. When the mapped target was overlapped with the transition state that leads to the major product, **4**(*si*), one of the ester groups of the DIPT ligand was found to be in close proximity (1.8−2.2 Å between carbonyl carbons, Figures 12b and 13b) to the first few probe clusters (those with the most favorable interaction energies). The carbonyl oxygens of these probes are oriented toward the aldehydic hydrogen in a manner similar to that of the DIPT ester proximal to the aldehyde. The distance between the aldehyde H of the transition state and the carbonyl O of the most stable methyl acetate probe is 2.68 Å (2.61 Å for the most stable methyl formate probe), indicating that a stabilizing interaction (sum of vdW radii for H and O = 2.72 Å) between these groups was found with the functionality mapping. This interaction reproduces one of the favorable interactions found in the tartrate ligand series. These same probes also reproduce the antiparallel arrangement between the carbonyl groups of the proximal DIPT ester and the aldehyde in the transition state. The occurrence of the probes near the other ester group of the DIPT ligand is sparse, which is consistent with the apparent lack of interactions from this ester in transition state calculations.[33]

We speculate that a ligand which places a carbonyl group closer to the position of the *formate 1* in Figure 13b would effect a more selective reaction. In line with this hypothesis, we have found that the corresponding carbonyl group of tartramide derived auxiliaries, such as that shown in **6**(*si*), is in fact closer to the calculated optimum of *formate 1* (Figure 14). These tartramide auxiliaries were designed to act as conformationally restricted analogues of the diisopropyl tartrate derivatives.[32] Roush proposed that the tartramides would be less conformationally flexible than the corresponding tartrates and that the auxiliary carbonyl would not be able to shift away from the cyclic transition state.[32,33] As such the key interactions differentiating the *si* vs *re* transition structures would be optimized for **6** relative to **4** (see Figure 11). The higher selectivity of the auxiliary from **6** (R = Bn) compared to that of **4** (DIPT) in several allylation reactions (85 vs 71% ee for PhCHO, 97 vs 87% ee for cHxCHO)[32] supports this proposal. On the basis of the functionality map shown in Figure 14, we propose that the eight-membered ring of the tartramides *also serves to position the stereodiscriminating carbonyl closer to the optimal site of interaction* in **6**(*si*) compared to the

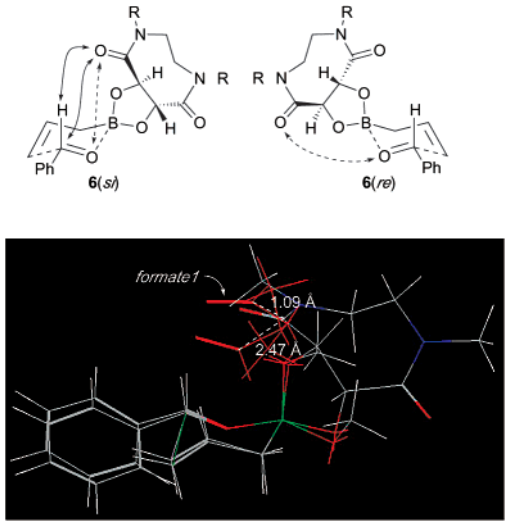

FIGURE 14. Top two clusters from functionality mapping of target **D**(*si*) with methyl formate probes. Target **D**(*si*) is overlaid with **6**(*si*).

tartrate ester in **4**(*si*) and that this placement may also play a role in magnifying the enantioselection.

Roush has reported that the stereoselective allylation reaction with the allyl boronate derived from (−)-2,3-butanediol was much less selective than that derived from DIPT (Figure 11b). For example, in the addition of (−)-2,3-butanediol allyl boronate to benzaldehyde 17% ee (*S*) was observed while in the addition of (+)-DIPT allyl boronate to benzaldehyde 71% ee (*S*) was observed.[30a] For (−)-2,3-butanediol, the methyl substituents had been proposed as the stereodiscriminating groups. With the aim of determining if these methyl substituents directly interact with the allylation portions of the transition states, a methane functionality map of **D** (dimethoxyborane) was undertaken. Mapping with 200 methane probes yielded 10 clusters; however, methane groups were not found that matched the methyl substituents in the (−)-2,3-butanediol ligand.

To ensure that the methoxy groups of dimethyl borate transition state **D** were not preventing proper placement of the methane probes, target **E** with smaller hydrogen substituents on the boron was also examined (Table 3, entries 3 and 4). As noted in the case of functionality mapping for the Masamune dimethylborolane, the methane molecules spread more widely over the surface of the transition state compared to benzene or methyl formate probes (Figure 15, parts a and b). Even so, a greater proportion of the methane probes were found to occupy positions near the unsaturated elements of the transition state due to superior van der Waals interactions with these electron-rich centers. The interaction energies are in the range of ∼6 kJ/mol and these van der Waals interactions are weaker than the electrostatic interactions observed for methyl acetate and methyl formate.

Importantly, an overlay of the (−)-2,3 butanediol transition state **5**(*si*) leading to the major product with the functionality map of **E**(*si*) revealed that no methane groups are in close proximity to the two "stereodiscriminating methyl groups" of the ligand (Figure 15, parts a and c). Furthermore, the closest methane groups to the methyl substituents of the (−)-2,3 butanediol have *only very weak interactions with the transition state as indicated by their yellow color*. These results are consistent with the low stereochemical selectivity displayed by the (−)-2,3-butanediol reagent and with calculations of this system.[33] As illustrated in the methane functionality map, the stereodiscriminating methyl substituents in these compounds do not occupy positions in which highly favorable (i.e., stabilizing) interactions with the transition state are likely. An overlay of the (−)-2,3-butanediol transition state **5**(*re*) leading to the minor product with a functionality map of **E**(*re*) (Figure 15b,d) is very similar. The methane probes nearest to the ligand methyl substituents are about as close as for **E**(*si*) and are only weakly interacting as indicated by their yellow color. From these results, it appears that the methyl substituents of (−)-2,3-butanediol stabilize/destabilize[34] **5**(*si*) and **5**(*re*) to the same extent. Hence, the reaction proceeds to a similar extent via both pathways. Overall the results from the functionality mapping anticipate that (−)-2,3 butanediol would provide low selectivity in allylboration reactions since the "stereodiscriminating methyl groups" do not match with methane groups that undergo stabilizing interactions in **E**(*si*) or destabilizing interactions in **E**(*re*) (or vice versa).

Iminium Diels−Alder Reactions. Recently MacMillan et al.[35] reported that secondary chiral amines are selective catalysts for the enantioselective Diels−Alder reactions of α,β-unsaturated aldehydes (eq 3). The amine

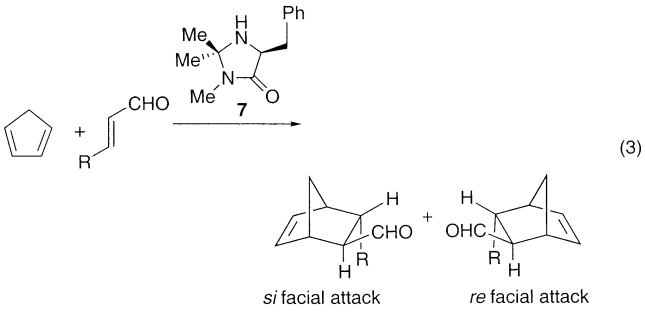

(3)

catalysts form iminium ion species in equilibrium with the α,β-unsaturated aldehydes; these iminium ions display a reactivity profile similar to Lewis acid coordinated α,β-unsaturated aldehydes and undergo facile Diels−Alder reactions. Among the chiral amine catalysts, **7** was found to be very effective, giving 93% ee of the (*S*) enantiomer for the exo adduct in the addition of cyclopentadiene to cinnamaldehyde. On the basis of calculations of the ground-state catalyst-aldehyde adduct using an MM3 force field, MacMillan et al. suggested that the benzyl group on the catalyst framework shields the *re* face of the dienophile, leaving the *si* face exposed to approaching diene. We applied functionality mapping to this example to investigate whether the favorable locations of the stereoselectivity determining phenyl groups in the catalysts can be predicted.

(34) If the methyl substituents destabilize one of the transition states (disfavorable interactions), then there should be no methanes from the functionality mapping matching the ligand methyl substituents in that transition state. This is not the case for (−)-2,3-butanediol since there is a similar level of matching for **5**(*si*) and the map of **E**(*si*) compared to **5**(*re*) and the map of **E**(*re*).

(35) Ahrendt, K. A.; Borths, C. J.; MacMillan, D. W. C. *J. Am. Chem. Soc.* **2000**, *122*, 4243.

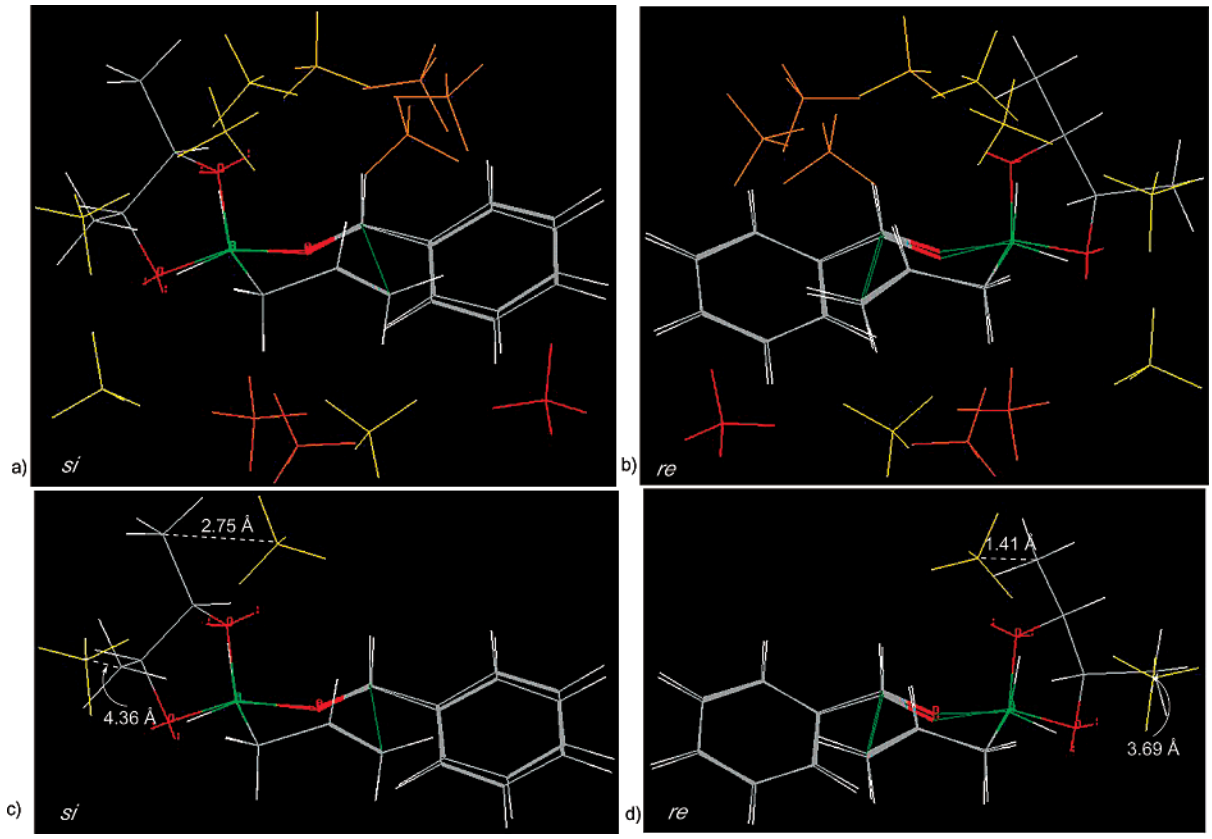

FIGURE 15. Functionality mapping of target **E** (dihydroborane) with methane probes. (a) Target **E**(*si*) is overlaid with **5**(*si*). (b) Target **E**(*re*) is overlaid with **5**(*re*). (c) Same as part a except only the two clusters closest to each methyl substituent of the chiral ligand are shown. (d) Same as part b except only the two clusters closest to each methyl substituent of the chiral ligand are shown.

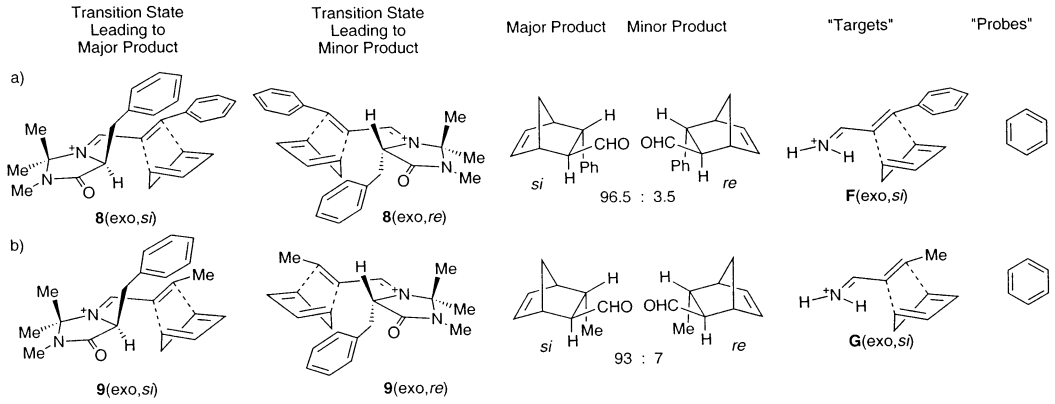

FIGURE 16. Iminium Diels−Alder transition states along with the corresponding targets and the probes used for the functionality mapping program.

As a first step in this analysis, we carried out Monte-Carlo conformational searches of the transition states for the catalyzed reaction illustrated in eq 3 using an MM2* force field.[11] To obtain all the possible transition state structures, four Monte-Carlo searches were performed with different starting points considering exo and endo approach as well as *si* and *re* facial attack of the diene. With this method, all reasonable transition states appear to have been located, including those arising from the s-cis and s-trans forms of the α,*β*-unsaturated iminium. A Boltzmann distribution of these transition structures at 298 K gives 87% ee (exo *S*), which is in good agreement with the experimental results (93% ee).[36] The Boltzmann distribution also reproduces the exo:endo ratio (calculated = 1.7:1, experimental = 1.3:1). In the most stable transition structure (Figure 16) the phenyl ring of the benzyl group sits above the olefinic *π*-bond. This reiterates the importance of the orientation of the phenyl ring of the ligand for this enantioselective reaction.[37] A *π*−*π* interaction between the olefinic *π*-unit and the phenyl

(36) For a further discussion as well as listings of transition state energies and structures, see the Supporting Information.

TABLE 4. Functionality Mapping Results for the Diels–Alder Transition States in Figure 16[a]

entry	target	relevant TS[b]	probe	no. of clusters[c]	populations; energies (kJ/mol) of the top five clusters 1st	2nd	3rd	4th	5th	energy range (kJ/mol)	RMSD in Å (energy in kJ/mol, cluster #)[d]
1	**F**(exo,*si*) MM2*	**8**(exo,*si*)	PhH	71	7; −22.27	9; −22.27	7; −22.27	10; −22.27	11; −22.27	−22.27 to −12.96	1.46 (−22.27, 1)
2	**F**(exo,*re*) MM2*	**8**(exo,*re*)	PhH	67	20; −22.03	13; −22.03	3; −22.03	7; −22.03	5; −22.03	−22.03 to −13.29	6.95 (−22.03, 1)
3	**F**(endo,*si*) MM2*	**8**(endo,*si*)	PhH	74	10; −21.94	7; −21.94	8; −21.94	1; −21.94	12; −21.94	−21.94 to −12.51	2.15 (−21.94, 1)
4	**F**(exo,*si*) HF/3-21G	**8**(exo,*si*)	PhH	64	13; −22.72	8; −22.72	6; −22.72	4; −22.72	11; −22.72	−22.72 to −13.83	1.81 (−16.55, 33)
5	**G**(exo,*si*) MM2*	**9**(exo,*si*)	PhH	76	3; −16.27	4; −16.27	9; −16.27	1; −16.27	5; −16.27	−16.27 to −11.55	2.59 (−15.33, 14) 2.80 (−16.27, 1) 3.68 (−14.47, 38)
6	**G**(exo,*si*) HF/3-21G	**9**(exo,*si*)	PhH	70	3; −15.68	8; −15.68	6; −15.68	6; −15.68	1; −15.68	−15.68 to −11.16	0.77 (−14.84, 22) 2.08 (−15.37, 7) 3.18 (−14.55, 34)

[a] 200 probes with a TNCG gradient and a convergence criterion of 0.01 kJ/(mol·Å) were used in all cases. [b] Corresponds to the transition state incorporating the relevant chiral auxiliary (see Figure 16) which is being compared to the target and its functionality map. [c] The high symmetry of benzene leads to mapping of up to 6 identical clusters having the same interaction energy. A 1.0 Å RMSD (heavy atoms) was used for clustering. [d] RMSD values comparing the 6 carbons of the closest benzene clusters with those of the phenyl stereodiscriminating group of the transition state from the third column. The interaction energy of these clusters and their rank, in terms of favorable interaction energy, are given in parentheses.

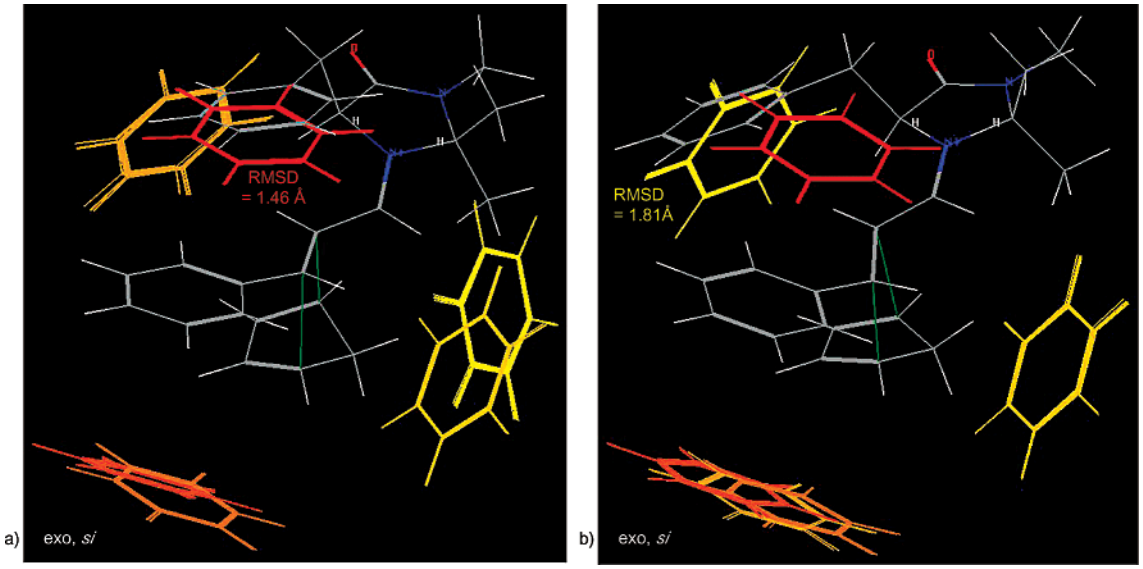

FIGURE 17. Functionality mapping of target **F**(exo,*si*) with benzene probes. Target **F**(exo,*si*) is overlaid with **8**(exo, *si*). (a) With the MM2* target, FUNMAP found 71 clusters (the first 40 are shown). (b) With the HF/3-21G target, FUNMAP found 64 clusters (the first 40 are shown).

ring of the benzyl ring may account for stabilization of this transition structure which is approximated by the MM2* force field with the van der Waals interaction parameters.

The cores of the iminium Diels–Alder transition states for cinnamaldehyde and crotonaldehyde, **F**(exo,*si*) and **G**(exo,*si*) respectively, were chosen as targets to study the interactions between these transition states and phenyl groups. With use of a benzene molecule as the probe, these targets were subjected to the functionality mapping analysis (Table 4).[15]

Functionality mapping of the MM2* transition state **F**(exo,*si*) revealed that the benzene probes concentrated to three general areas (Figure 17a). The most favorable position for the benzene ring over the surface of the target was above the alkene unit of the dienophile. The interaction energy of this arrangement is −22.3 kJ/mol. When overlapped with **8**(exo,*si*), which is the lowest energy transition state containing ligand **7**, these probes were found to be near the phenyl ring of the ligand (RMSD of the closest cluster to the phenyl group = 1.46 Å). If the interaction of the chiral ligand phenyl group with respect to the transition state is the key feature in determining reaction stereoselection, then less favorable overlaps should be seen between the functionality maps of the transition states leading to the minor product and the chiral ligand. This hypothesis was borne out as illustrated in the benzene functionality map of **F**(exo,*re*). In Figure 18a, the α,β-unsaturated iminium of this target is overlaid with the lowest energy transition state,

(37) The α,β-unsaturated iminium portion of the most stable transition structure is very similar to the most stable ground-state iminium structure identified by MacMillan et al. As a result, the rationale to explain the selectivity by using the transition structures is analogous to that invoked for the ground states (ref 35).

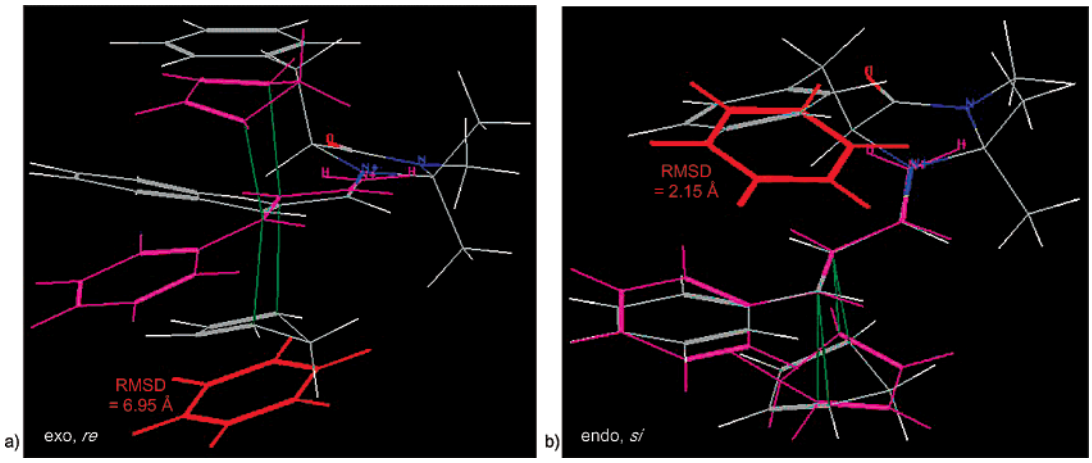

FIGURE 18. (a) Functionality mapping of MM2* target **F**(exo,*re*), which is shown in purple, with benzene probes (the 12 overlapping clusters with the best interaction energies are shown in red). The α,*β*-unsaturated iminium of **F**(exo,*re*) is overlaid with that of **8**(exo,*si*), which is shown in half-bond colors. (b) Functionality mapping of MM2* target **F**(endo,*si*), which is shown in purple, with benzene probes (the 11 overlapping clusters with the best interaction energies are shown in red). The α,*β*-unsaturated iminium of **F**(endo,*si*) is overlaid with that of **8**(exo,*si*), which is shown in half-bond colors.

8(exo,*si*), which leads to the major product. The benzene probes with the best interaction energies with **F**(exo,*re*) are quite distant from the phenyl ring of the ligand (RMSD of the closest cluster to the phenyl group = 6.95 Å). On this basis, the ligand would not be expected to stabilize this reaction pathway, which is consistent with the observed (exo,*si*):(exo,*re*) ratio of 96.5:3.5 for this reaction. Further functionality mapping of target **F**(endo,*si*) with benzene (Figure 18b) revealed that this reaction pathway does have a favorable interaction energy with a benzene in a position close to that of the phenyl ring of the catalyst (RMSD of the closest cluster to the phenyl group = 2.15 Å). This result is consistent with the low exo:endo selectivity of 1.3:1 exhibited by the catalyst. In other words, the phenyl substituent of the catalyst stabilizes both the (exo,*si*) and (endo,*si*) reaction pathways.

The MM2* transition structures for these Diels−Alder reactions were highly synchronous (both C−C bonds formed to a similar degree in the transition structure). Due to the polarized nature of the α,*β*-unsaturated iminium, such geometries are not expected. To obtain more reliable geometries, we carried out HF/3-21G calculations using the MM2* structures as initial guesses.[12] Asynchronous transition states were obtained in which the bond to the *β*-carbon was formed to a greater degree than the bond to the α-carbon. In addition, the HF/3-21G transition states were somewhat earlier as characterized by the relatively planar cyclopentadiene ring. Interestingly, the orientation of the phenyl ring of the ligand is shifted away from the optimal position for a $\pi-\pi$ interaction. This alternate, more stable transition structure apparently arises from a C(sp^2)H−π interaction between the alkene hydrogen and the phenyl ring. Nevertheless, the phenyl ring still blocks the *re* facial approach of the diene and the HF/3-21G transition states were strikingly similar to the corresponding MM2* transition states (Figure 17).

On the basis of similar transition structure geometries found for this reaction with MM2* and HF/3-21G, functionality mapping of the latter was also investigated. In this case, the **F**(exo,*si*) HF/3-21G geometry was introduced and the structure was held fixed while a functionality map was generated with an MM2* force field.[13,15] The resultant functionality map (Figure 17b) was very similar to that from the MM2* geometry (Figure 17a). In both cases, the probes with the most favorable interaction energy (red phenyl groups in Figure 17) were found parallel to the alkene of the α,*β*-unsaturated iminium. This outcome occurs because $\pi-\pi$ and CH−π interactions are poorly represented by the MM2* force field. As a result, van der Waals interactions between benzene probes and the alkene π-system are preferred over those between benzene probes and the C(sp^2)H. When a force field (MM3*) that is parametrized for $\pi-\pi$ and CH−π interactions[38] was employed, the functionality mapping did reproduce the position of the phenyl group in the **8**(exo,*si*) HF/3-21G structure. Interestingly, when the MM2* functionality map of **F**(exo,*si*) HF/3-21G was overlapped with the **8**(exo,*si*) HF/3-21G transition state containing the chiral ligand, a few probes were found near the phenyl ring of ligand **7** (RMSD of the closest cluster to the phenyl group = 1.81 Å) albeit with lower interaction energies (−16.6 vs −22.7 kJ/mol) compared to phenyl rings found over the π-bond. Use of the **G**(exo,*si*) HF/3-21G transition structure as a target was also successful (see Figure 19b). These results indicate that rapid molecular mechanics functionality mapping can be combined with more accurate quantum mechanical transition states.

When the phenyl group of the cinnamaldehyde substrate is replaced with a methyl group (crotonaldehyde), the selectivity of the Diels−Alder reaction drops to 93:7 from 96.5:3.5 with the same catalyst (**7**). To determine whether the functionality mapping possesses sufficient precision to anticipate this difference in selectivity, a benzene functionality map of the MM2* version of **G**(exo,*si*) was generated (Figure 19). Examination of Figure 19 reveals that the most stable red cluster is positioned further away from the crotonaldehyde iminium ion compared to the cinnamaldehyde variant shown in Figure 17a. As a result, the optimal position for a

(38) Lii, J.-H.; Allinger, N. L. *J. Am. Chem. Soc.* **1989**, *111*, 8576.

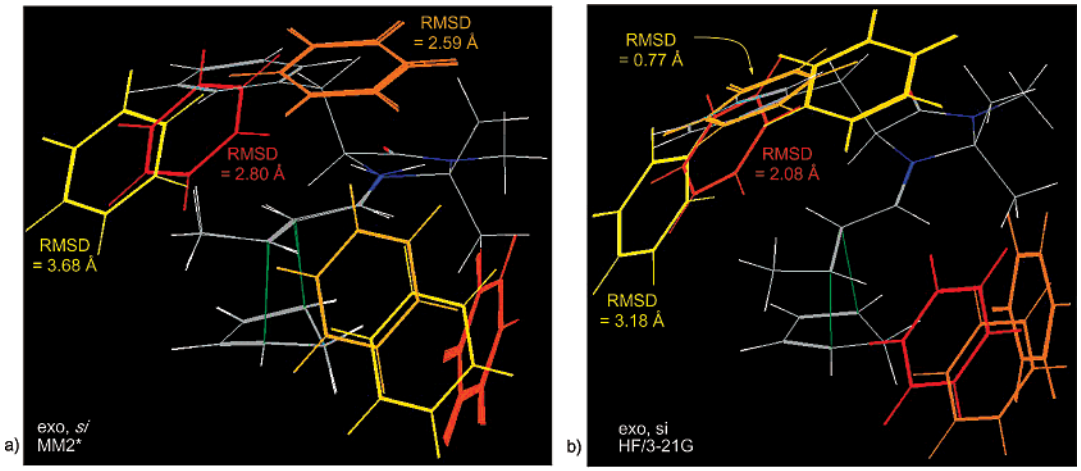

FIGURE 19. Functionality mapping of target **G**(exo,*si*) with benzene probes. Target **G**(exo,*si*) is overlaid with **9**(exo,*si*). RMSD values between the clusters and the ligand phenyl substituent are shown. (a) With the MM2* target, FUNMAP found 76 clusters (the first 40 are shown). (b) With the HF/3-21G target, FUNMAP found 70 clusters (the first 40 are shown).

benzene group predicted in **G**(exo,*si*) is *further away* from the ligand phenyl substituent of the lowest energy **9**(exo,*si*) crotonaldehyde transition structure (RMSD = 2.80 Å) relative to the corresponding **8**(exo,*si*) cinnamaldehyde transition structure (RMSD = 1.46 Å). This result indicates that the ligand does not perform as well at stabilizing the **9**(exo,*si*) crotonaldehyde transition structure compared to the corresponding **8**(exo,*si*) cinnamaldehyde transition structure, which is consistent with the lower selectivity observed for crotonaldehyde. The smaller difference between the (exo,*si*) and (exo,*re*) RMSD values of **G** (Δ = 4.24 Å) compared to those of **F** (Δ = 5.49 Å) is also in line with this hypothesis.

Concluding Remarks

The functionality mapping method described can be used with a variety of functional group probes to determine the optimal placement of ligand substituents with respect to a transition structure. These functionality mapping tools can be used to better understand the nonbonded interactions of ligand functional groups in transition states leading to chiral products. By quantifying the positions and energy stabilization afforded by specific nonbonding interactions, it is possible to determine if a chiral ligand imparts the observed selectivity by stabilizing one reaction pathway, by destabilizing a reaction pathway, or by a combination of both. Orientational as well as positional information about potential functional groups is readily obtained. The importance of such suitably oriented functionalized substituents (stereodiscriminating groups) to the high enantioselection imparted by a series of chiral ligands has been corroborated by the functionality mappings of the respective transition states.

In addition to its utility as an analytical tool, the functionality mapping can also be used to explore starting points for de novo ligand design. Suitably oriented functional groups for a target reaction could be identified and then incorporated into a structurally rigid molecular framework. Such an approach may allow the optimization of known ligands in established processes or the design of chiral ligands for new processes. Overall the functionality mapping is expected to complement other methods of chiral ligand design by allowing a thorough assessment of nonbonding interactions in transition state models.

Acknowledgment. Financial support was provided by the National Institutes of Health (GM59945). We thank Giorgio Lauri for helpful discussions and for providing the FUNMAP program. Computational support for the Hartree−Fock calculations was provided by the NCSA in the form of a supercomputing time allotment. We thank Giorgio Lauri for assistance in the preparation of the cover graphic.

Supporting Information Available: The CPU times for representative functionality mapping runs and functionality mapping results with different gradients are given along with details of the transition state calculations. This material is available free of charge via the Internet at http://pubs.acs.org.

JO020401S